Rotational Encoding of C-arm Fluoroscope with Tilt Sensing Accelerometer

Victor Grzeda and Gabor Fichtinger

Queen's University, Kingston, ON, Canada
v.grzeda@queensu.ca, gabor@cs.queensu.ca

Abstract. *Purpose*: Accurate, practical, and affordable joint encoding on legacy C-arm fluoroscopes is a major technical challenge. Conventional pose tracking methods, like optical cameras and radiographic fiducials, are hampered by significant shortcomings. *Methods*: We propose to retrofit legacy C-arms with a tilt sensing accelerometer for rotation encoding. Our experimental setup consists of affixing an accelerometer to a full scale C-arm with a webcam as an alternative to X-ray imaging for this feasibility research. Ground-truth C-arm poses were obtained from the webcam that tracked a checkerboard plate. From these we constructed a series of angle and structural correction equations that can properly relate the accelerometer angle readings to C-arm pose during surgery and compensate for systematic structural C-arm deformations, such as sagging and bending. *Results*: Real-time tracking of the primary and secondary angle rotations of the C-arm showed an accuracy and precision of less than 0.5 degrees in the entire range of interest.

Keywords: fluoroscopy, C-arm, tracking, encoding, accelerometer.

1 Introduction

C-arm fluoroscopes are ubiquitous in computer-assisted interventions. They are versatile, compact, and mobile real-time X-ray imaging devices. The basic use of a C-arm is to acquire 2D X-ray images that can be reconstructed into three-dimensional representation. The reconstruction process requires that the relative poses of the 2D projection images must be known. Accurate, practical, and affordable C-arm pose tracking is a major technical challenge in using manually operated and un-encoded conventional C-arm fluoroscopes.

The motivation for this project is intra-operative implant reconstruction in prostate cancer brachytherapy [3]. C-arm images are acquired of the implanted prostate, followed by a 3D reconstruction of implants relative to the prostate gland and other surrounding structures observed in ultrasound. Then dosimetry is computed and the remainder of the implant procedure is re-optimized. For a successful implant reconstruction, the C-arm pose needs to be recovered with ideally less than 1° error [3,4,6]. Various constraints imposed by potential collisions with patient, operating table, and standard brachytherapy instrumentation limit the usable range of the C-arm to about a 30° cone in the canonical vertical position (Figure 1, *left*).

T. Jiang et al. (Eds.): MICCAI 2010, Part III, LNCS 6363, pp. 424–431, 2010.

Conventionally, C-arm pose tracking takes one of two forms. External tracking uses a dynamic reference body that is attached to the C-arm and sensed by optical cameras to recover the pose [5]. Optical cameras can recover the C-arm pose accurately and are resistant to common problems that plague C-arms such as wheel motion and structural deformation. However, shortcomings lie in the need for direct line of sight between the reference body and the camera, leading to a complex, labor-intensive, and ultimately costly setup for most care facilities. Image-based tracking uses a radio-opaque fiducial placed in the field of imaging [3,4,7]. The precision-machined fiducial has known geometry allowing for the C-arm pose to be computed relative to the fiducial in each individual fluoroscopic image. While fiducial tracking is inexpensive, potentially accurate, and universally usable for any C-arm, it also has disadvantages. The fiducial occupies valuable real estate in the image, forcing the prostate to be positioned toward the edge of the detector, where image distortion is larger and may demand online distortion correction. Equally as important, the image needs careful processing and the fiducial must be segmented, which has been a singular point of failure in the clinical procedure [3,4]. Accelerometers have been considered for full position tracking, but those studies revealed accumulating drift error in measuring the pose [8], which thus far has prohibited the application of accelerometers in surgical guidance.

In the operating room, the brachytherapy crew is under incessant pressure to complete the image acquisition in minimum time. In such haste, more often than not the C-arm is still in motion when the X-ray image is acquired. Even if the joints look stationary, the C-arm keeps rocking on the rubber wheels and the gantry is swinging. Accelerometers detect these motions and thus enable us to gait the image acquisition accordingly. If one can guarantee stationary wheel and gantry positions, then the full pose the C-arm image can be recovered from joint encoders alone, assuming that the C-arm's kinematics had been obtained *a priori* in a one-time calibration.

We revisited the use of accelerometers that are well-suited to accurately indicate transient motion while they can be configured as tilt sensors. Preliminary bench work explored the feasibility of this approach on a crudely built and downscaled C-arm analogue [1]. A plethora of technical obstacles arises in translating this approach to a full scale clinical C-arm. This paper explains these barriers and having overcome them to achieve affordable and clinically accurate rotational encoding on a full scale C-arm fluoroscope, with the use of an accelerometer configured as tilt sensor.

2 Methodology

2.1 Calibration

The accelerometer angle encoding technique requires a one-time calibration step to relate the raw accelerometer angle to the C-arm pose. The linear workflow consists of several steps: (1) Mount the accelerometer on the C-arm; (2) Place C-arm tracking fiducial in the field of view; (3) Acquire test images while logging the initial rotation pose from the accelerometer; (4) Compute reference poses using the fiducial; (5) Compute the offset for both primary and secondary C-arm angles; (6) Confirm the accuracy of calibration on subset of independent measurements left out from the calibration computations. Preliminary investigation of this technique on a down-scaled

C-arm analogue was promising [1], but it revealed major uncertainties in translating this approach to a full scale C-arm. One such uncertainty is the effect of wheel motion. Mobile C-arms use wheel locks to secure the device in place, but these locks are not perfect. During rotational movement the C-arm tends to experience rocking and swinging motions that affect the pose of the image. In our case, since an accelerometer is used, real-time analysis of acceleration readings can detect acceleration spikes. These spikes indicate rapid motion changes (rocking, swaying) of the C-arm. By continuously monitoring for the spike to subside (steady state) a *go-ahead* signal can be flagged to indicate when images can be captured avoiding added error to the image pose.

The main area of concern is the deformation of the C-arm structure due to the force of gravity acting on the heavy X-ray source and detector. This deformation could cause an unaccounted for offset that would lead to inaccurate tracking of the C-arm pose. We mounted a webcam on a full scale C-arm unit, shown in Figure 1, *right*. Using webcam allows for conducting tests without exposure to ionizing radiation.

For the technique to be applied properly requires two key parameters that are determined from the C-arm and accelerometer combination. The first are Angle Correction Equations (ACEs) that account for the initial offset between the raw accelerometer angle readings to the C-arm pose. The second is a series of Structural Compensation Equations (SCEs) that account for the deformation of the C-arm during different rotational poses. This technique requires a one-time calibration of the C-arm to determine the ACEs and SCEs. These equations remain valid for continued use of the C-arm given that the accelerometer remains fixed on the gantry.

Our methodology of acquiring a series of test images and modeling the structural deformation of the C-arm is similar to Gorges et al [2]. Their work involved modeling the deformation as changes to the intrinsic/extrinsic parameters of the C-arm. Then they used cost functions to optimize the parameters to account for the deformations.

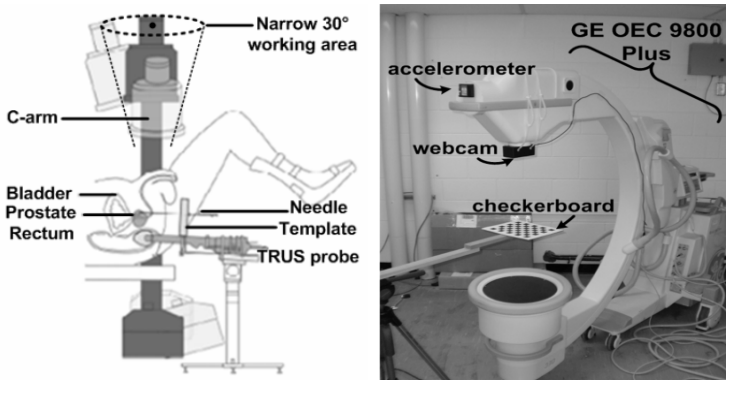

Fig. 1. (*Left*) Typical ultrasound guided brachytherapy setup with a C-arm operating in a narrow range. (*Right*) Full scale experimental setup with the accelerometer mounted on top and the webcam underneath the X-ray source. More details of devices can be found in [1].

2.2 Angle Correction Equations

The Angle Correction Equations (ACEs) quantify the offset between the webcam C-arm pose and the accelerometer angle readings. Generating the ACEs involves analyzing the differences between the initial accelerometer angle reading and ground-truth pose angle. In an actual clinical application, the ground truth pose will be computed using a radio-opaque fluoroscope tracking fiducial such as the one developed by Jain et al [3]. In our experimental setup, we applied optical imaging with a webcam mounted externally on the gantry over the exit point of the X-ray source. The webcam tracked a checkerboard pattern that provided the ground-truth C-arm poses of the 2D images through standard camera calibration techniques.

To determine the initial offset a set of test images were taken, in step-and-shoot mode, at the angles [0° ±5° ±10° ±15° ±20° ±25° ±30°] using the initial accelerometer angle reading for the primary angle (PA) and secondary angle (SA) independently. These were chosen to give enough separation between angles with a wide range to account for changes in the C-arm motion, as well as encapsulating the clinical angle limitation motivating this work. It should be noted that acquiring more angles could help to improve modeling, but when this will be used in X-ray imaging that would increase radiation exposure. Further testing will try to reduce the angle set and examine if proper tracking can be still achieved. Next, the actual pose angles of the images were computed and the differences calculated. By graphically visualizing the differences (Figure 2), best fit methods were applied creating the ACEs.

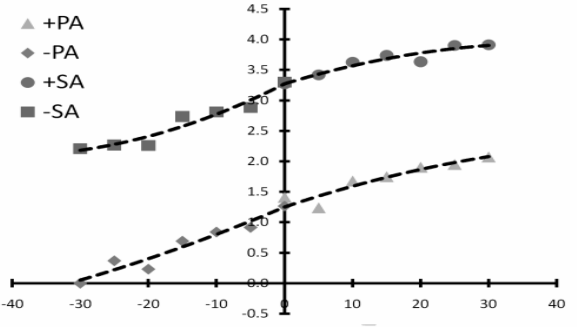

Fig. 2. A plot of the differences and fitted lines creating the Angle Correction Equations

The *Eq.1* and *Eq. 2* are the resulting ACEs. Interestingly, the structure of the C-arm creates non-linear trends that required piecewise functions for modeling. The intercept values in the functions were set the same to avoid sudden shifts in the output during sign changes of the angles when the accelerometer is operating.

Let x represent the initial *PA* then the new output angle

$$PA^{*} = \begin{cases} -0.0003 \cdot x^{2} + 1.037 \cdot x + 1.250 & x \geq 0 \\ 0.0002 \cdot x^{2} + 1.047 \cdot x + 1.250 & x < 0 \end{cases}, \quad (1)$$

Let z represent the initial SA then the new output angle

$$SA^* = \begin{cases} -0.0004 \cdot z^2 + 1.034 \cdot z + 3.270 & x \geq 0 \\ 0.0007 \cdot z^2 + 1.051 \cdot z + 3.270 & x < 0 \end{cases}. \quad (2)$$

2.3 Structural Compensation Equations

The full scale C-arm presented a major challenge due to the significant structural deformation. An initial test of the ACEs (*Eq. 1* and *Eq. 2*) showed that proper pose tracking was achieved, but only for independent angle rotations. Figure 3, displays a chart that illustrates the problem.

ROTATION DEG°	PRIMARY ANGLE 30	25	20	15	10	5	0	-5	-10	-15	-20	-25	-30	
SECONDARY ANGLE 30							-1.29 29.99							
25		24.07 27.68					-1.19 24.92					-25.94 26.86		
20			18.91 21.38				-1.12 20.05				-20.86 21.19			
15				14.08 15.58			-0.66 15.09			-15.67 15.54				
10					9.14 10.15		-0.51 10.05		-10.70 10.68					
5						4.60 4.98	-0.38 5.18	-5.64 5.53						
0	29.75 -0.66	24.59 -0.72	19.77 -0.66	14.77 -0.69	9.58 -0.65	4.68 -0.62	-0.23 0.12	-5.13 0.44	-10.14 0.44	-14.88 0.00	-20.06 -0.31	-25.09 -0.77	-29.95 -1.22	PA SA
-5						4.96 -4.95	0.02 -4.71	-5.07 -4.28						
-10					10.05 -9.66		0.26 -9.68		-9.85 -9.59					
-15				15.32 -15.43			0.55 -14.62			-14.90 -15.29				
-20			20.27 -21.28				0.46 -19.68				-19.99 -21.75			
-25		25.02 -27.78					0.38 -24.85					-24.71 -28.40		
-30							0.43 -30.23							

Fig. 3. [*inside cells* – actual C-arm pose angles: PA (shaded) | SA below || *outside border* – C-arm pose positions using ACEs accelerometer readings] The chart portrays that PA and SA are accurately tracked independently, but not very well simultaneously

To correct this problem required a different approach than a simple offset correction, like the ACEs. The fact is the ACEs did accurately track the PA and SA independently. What is posited here is that the structural deformation of the C-arm has dependency on PA and SA. As the rotation angle of the source or detector moves further from vertical the effects of gravity become greater. This dependence on the pose angle of the C-arm required us to compensate for the structural deformation, thus creating the Structural Compensation Equations.

The Structural Compensation Equations (SCEs) were formulated by reprocessing the test images that created the ACEs, with additional diagonal combinations of PA

and SA, shown in Figure 3. The errors were computed and zeroed to visualize the deformation for both the PA and SA separately. Line fitting was applied to the differences to create a series of equations, shown in Figure 4.

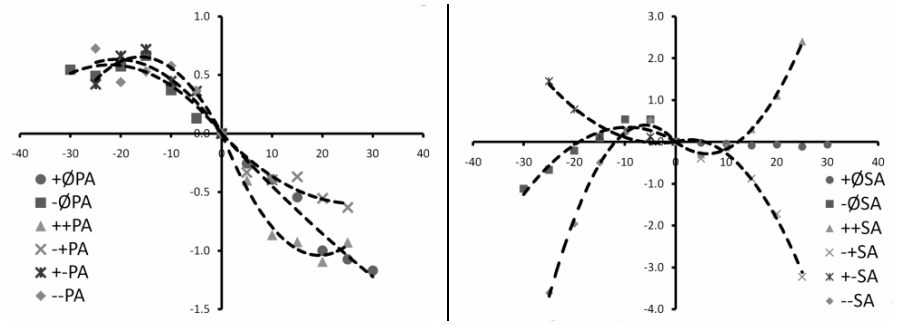

Fig. 4. The visualization of the C-arm deformations with accompanying best fit lines for PA (*left*) and SA (*right*). The horizontal axis represents the rotational angle, while the vertical indicates the amount of deformation.

The plots show that a significant amount of deformation exists and by zeroing the error creates a single starting position to make compensation easier to handle. A threshold value of τ helped to control when to activate compensating depending on the current angle values for PA and SA. The equations are piecewise functions separated into ±PA and ±SA quadrants shown here:

Let $w = PA^*$ and $x = SA^*$ then the compensated angle

$$PA^{\dagger} = \begin{cases} w + (0.0002 \cdot x^2 - 0.047 \cdot x) & x \geq 0 \\ w + (-0.0012 \cdot x^2 - 0.053 \cdot x) & x < 0 \\ w + (0.0028 \cdot x^2 - 0.107 \cdot x) & w > \tau, x > \tau \\ w + (0.0008 \cdot x^2 - 0.045 \cdot x) & w < -\tau, x > \tau \\ w + (-0.0025 \cdot x^2 - 0.081 \cdot x) & w > \tau, x < -\tau \\ w + (-0.0015 \cdot x^2 - 0.061 \cdot x) & w < -\tau, x < -\tau \end{cases}, \tag{3}$$

$$SA^{\dagger} = \begin{cases} x & w \geq 0 \\ x + (-0.0038 \cdot w^2 - 0.073 \cdot w) & w < 0 \\ x + (0.0075 \cdot w^2 - 0.093 \cdot w) & w > \tau, x > \tau \\ x + (0.0030 \cdot w^2 + 0.019 \cdot w) & w < -\tau, x > \tau \\ x + (-0.0065 \cdot w^2 - 0.038 \cdot w) & w > \tau, x < -\tau \\ x + (-0.0113 \cdot w^2 - 0.135 \cdot w) & w < -\tau, x < -\tau \end{cases}. \tag{4}$$

3 Results and Discussion

In order to characterize how accurately the ACEs and SCEs tracked the webcam C-arm pose we performed a series of tests. For the first test, the test image angles were changed for PA and SA to [0° ±2° ±6° ±10° ±14° ±18° ±22° ±26°] for both independent and combinational rotation of PA and SA. This change was made to contain different angles than the ones used to create the equations, so that they can be independently evaluated. The results, in chart form, are shown Figure 5.

ROTATIONS	PRIMARY ANGLE														
SECONDARY ANGLE / DEG°	26	22	18	14	10	6	2	0	-2	-6	-10	-14	-18	-22	-26
26								0.04 26.26							
22		22.34 21.45						0.11 22.20						21.74 21.55	
18			18.34 17.74					0.17 18.39					17.99 17.91		
14				14.47 13.91				0.30 14.22				13.89 13.99			
10					10.35 9.86			0.04 10.36			9.78 10.24				
6						6.25 5.61		0.14 6.23		6.16 6.37					
2							2.05 1.68	0.07 2.05	2.06 2.21						
0	26.04 -0.30	21.87 -0.30	18.04 -0.43	14.02 -0.68	10.12 -0.56	6.02 -0.77	2.31 -0.61	0.29 0.20	1.69 0.25	5.87 0.42	9.64 0.27	13.69 0.22	17.17 0.04	21.62 0.02	25.70 0.07
-2							2.08 -1.91	0.12 -1.40	2.04 -1.84						
-6						5.82 -5.98		0.15 -5.72		6.08 -5.71					
-10					9.94 -9.94			0.06 -9.49			9.79 -9.70				
-14				13.66 -13.71				0.17 -13.87				14.03 -13.56			
-18			17.82 -17.38					0.15 -18.07					18.22 -17.33		
-22		21.67 -21.36						0.10 -21.88						22.07 -21.20	
-26								0.02 -25.99							

Fig. 5. Results from using the ACEs and SCEs

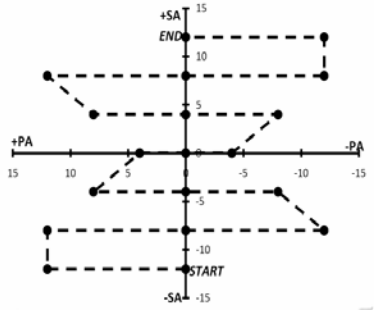

ROTATIONS	PRIMARY ANGLE						
SECONDARY ANGLE / DEG°	12	8	4	0	-4	-8	-12
12				0.12 12.18			11.72 12.05
8	12.45 8.09			0.11 8.20			11.78 8.22
4		8.38 4.10		0.17 4.11		7.72 4.06	
0			4.23 0.14	0.16 0.02	3.83 0.14		
-4		8.10 4.17		0.13 4.10		7.55 4.19	
-8	11.76 8.32			0.45 8.09			11.54 7.99
-12	11.81 12.36			0.39 12.55			

Fig. 6. The path of C-arm where the dots are the locations that the images acquired

The chart in Figure 5 suggests that, using the ACEs and SCEs the C-arm pose was tracked with an average error of $\mu = 0.11°$ and standard deviation of $\sigma = 0.21°$ for PA.

While for SA an average error of $\mu = 0.08°$ and standard deviation of $\sigma = 0.36°$. A second test was performed to show if the C-arm pose can be tracked when subjected to sequential rotation path with results shown in Figure 6.

We achieved C-arm rotation encoding by using accelerometer as tilt sensor, with an accuracy and precision of less than 0.5°. This was made possible by introducing the Structural Compensation Equations (SCEs). These equations worked in tandem with the Angle Correction Equations (ACEs) to compensate for the inherent structural deformation of the C-arm experienced at different rotational poses. We received excellent rotation encoding for the entire clinically relevant C-arm working range in prostate brachytherapy, our driving clinical application.

For other clinical application areas where the working range is larger, it is evident from Figure 5 that accelerometer tracking is not perfect where accuracy starts to waiver at the larger combined rotational poses. This effect could be attributed to the threshold values for when the SCEs need to start compensating for the structural deformation. The values control the activation of these equations, but it is not clear on when they should start. In brachytherapy, the SCEs were created by zeroing the offset, but it may be possible to start monitoring for changes farther away from the origin. The reasoning behind this is that the lower angles about the vertical axis would have less deformation caused by gravity and could still be within the ACEs capability of tracking. The next step in continuing research will be to determine a threshold location rather than a singular conditional value.

In conclusion, C-arm rotation tracking was successful with using the tilt-sensing capabilities of accelerometers. Work continues to implement this concept on fully functional X-ray imaging C-arms, with the ultimate goal of clinical deployment of an accurate, inexpensive and easy-to-use rotation technique in prostate brachytherapy.

References

[1] Grzeda, V., Fichtinger, G.: C-arm rotation encoding with accelerometers. International Journal of Computer Assisted Radiation and Surgery 5(4), 385–391 (2010)

[2] Gorges, S., Kerrien, E., Berger, M.-O., et al.: Model of a Vascular C-Arm for 3D Augmented Fluoroscopy in Interventional Radiology. In: Duncan, J.S., Gerig, G. (eds.) MICCAI 2005. LNCS, vol. 3750, pp. 214–222. Springer, Heidelberg (2005)

[3] Jain, A.K., Deguet, A., Iordachita, I., et al.: Intra-operative Guidance in Prostate Brachytherapy Using an Average Carm. In: Ayache, N., Ourselin, S., Maeder, A. (eds.) MICCAI 2007, Part II. LNCS, vol. 4792, pp. 9–16. Springer, Heidelberg (2007)

[4] Lee, J., Liu, X., Jain, A.K., et al.: Prostate brachytherapy seed reconstruction with Gaussian blurring and optimal coverage cost. IEEE Trans Med. Imaging 28(12), 1955–1968 (2009)

[5] Peters, T., Cleary, K. (eds.): Image-Guided Interventions: Technology and Applications. Springer, Heidelberg (2008)

[6] Tubic, D., Zaccarin, A., Beaulieu, L., Pouliot, J.: Automated seed detection and three-dimensional reconstruction. II. Reconstruction of permanent prostate implants using simulated annealing. Medical Physics 28(11), 2272–2279 (2002)

[7] Yao, J., Taylor, R.H., Goldberg, R.P., et al.: A C-arm fluoroscopy-guided progressive cut refinement strategy using a surgical robot. Comput. Aided Surg. 5(6), 373–390 (2000)

[8] Nikbakht, S., Mazlom, M., Khayatian,: Evaluation of solid-state accelerometer for positioning of vehicle. In: IEEE Int'l. Conference on Industrial Technology, pp. 729–733 (2005)